# An injectable and coagulation-independent Tetra-PEG hydrogel bioadhesive for post-extraction hemostasis and alveolar bone regeneration

Gang He [a,1], Yiwen Xian [a,1], Huajun Lin [b], Chengcheng Yu [b], Luyuan Chen [b], Zhihui Chen [b], Yonglong Hong [b,***], Chong Zhang [a,**], Decheng Wu [a,*]

[a] Guangdong Provincial Key Laboratory of Advanced Biomaterials, Department of Biomedical Engineering, Southern University of Science and Technology, No. 1088 Xueyuan Avenue, Nanshan District, Shenzhen, Guangdong, 518055, China
[b] Department of Maxillofacial Surgery, Shenzhen Hospital, Southern Medical University, No. 1333 New Road, Baoan District, Shenzhen, Guangdong, 518101, China

## ARTICLE INFO

## ABSTRACT

Effective control of post-extraction hemorrhage and alveolar bone resorption is critical for successful extraction socket treatment, which remains an unmet clinical challenge. Herein, an injectable Tetra-PEG hydrogel that possesses rapid gelation, firm tissue adhesion, high mechanical strength, suitable degradability, and excellent biocompatibility is developed as a sutureless and coagulation-independent bioadhesive for the management of extraction sockets. Our results demonstrate that the rapid and robust adhesive sealing of the extraction socket by the Tetra-PEG hydrogel can provide reliable protection for the underlying wound and stabilize blood clots to facilitate tissue healing. *In vivo* experiments using an anticoagulated rat tooth extraction model show that the hydrogel significantly outperformed clinically used cotton and gelatin sponge in hemostatic efficacy, wound closure, alveolar ridge preservation, and *in situ* alveolar bone regeneration. Histomorphological evaluations reveal the mechanisms for accelerated bone repair through suppressed long-term inflammation, elevated collagen deposition, higher osteoblast activity, and enhanced angiogenesis. Together, our study highlights the clinical potential of the developed injectable Tetra-PEG hydrogel for treating anticoagulant-related post-extraction hemorrhage and improving socket healing.

## 1. Introduction

Dental extractions become unavoidable in some cases, including caries, periodontal diseases, traumatic injuries, orthodontic and prosthodontic treatments, root fractures, and endodontic failures [1,2]. Surgical repair of extraction wound is routinely performed by closure of the defect with sutures or applying mechanical compression including the use of medical cotton balls, gauze, or gelatin sponge. However, despite being the standard of care, these methods generally have inherent drawbacks. Suturing is technically challenging and time-consuming and can cause local tissue damage [3–5]. Meanwhile, traditional dressings cannot provide durable and effective protection

against complex oral environments for wound hemostasis and healing, resulting in several adverse events, including secondary bleeding, dry socket, delayed wound repair, and infection [6,7]. Moreover, unexpected post-extraction bleeding arising from local and systemic factors is frequently encountered (i.e., up to 26% incidence), which is often challenging to manage with the existing hemostatic agents [8,9]. These situations become more urgent and life-threatening for patients on long-term anticoagulant therapy, especially considering that dental surgeries are nowadays recommended to be carried out without reducing or discontinuing anticoagulant therapy to prevent the recurrence of thromboembolism [10,11]. As a result, developing new strategies for socket wound care to offer rapid and coagulation-independent

hemostatic sealing is highly desirable but remains a critical challenge.

The physiologic or pathological bone remodeling process following tooth extraction can lead to alveolar bone resorption, which has been reported to be 29–63% horizontal bone loss within the first 6 months, resulting in a significant compromised function and esthetics outcomes of the subsequent dental implant rehabilitation [12,13]. To minimize this inevitable complication, the application of graft materials, barrier membranes, and bioactive agents, either alone or in combinations, have been proposed to guide bone regeneration in terms of maintaining adequate ridge volume and enhancing bone formation [14–16]. However, these reconstructive technologies display limitations, such as secondary lesions, short supply, risk of disease transmission or immunogenic reaction, and poor long-term results [17,18]. More recently, several new biomaterial scaffolds have been developed [19–23]. For example, Niu et al. developed a polyphosphate-crosslinked collagen scaffold for promoting bone regeneration [19]. Yin et al. designed a porous shape memory scaffold with self-adaptive and anti-bacterial functions to fill the socket and boost alveolar bone regeneration [20]. Liu et al. reported a supramolecular photothermal cascade nanoreactor based on chitosan-modified palladium nano-cube, glucose oxidase, and ferrous iron for accelerating the healing of infected tooth-extraction wounds [23]. Although improvement in alveolar bone repair is achieved, particular concerns with these features of scaffolds are their poor fluid-tight sealing, and/or inadequate mechanical performance, and even potential toxic by-products, making them insufficient for effective bleeding control and wound protection in the dynamic and wet oral environment.

In light of these shortcomings, the clinical needs have motivated tremendous efforts to develop wound dressings that feature superior biocompatibility, rapid bleeding control, and excellent alveolar bone reservation for tooth extraction treatment. Hydrogel-based bioadhesives, especially injectable hydrogels, have emerged as a promising option for wound management, owning to their structural similarity to the extracellular matrix, tunable physicochemical properties, and ability to fill the deep and complex-shaped voids with minimally invasive surgery [3,24–32]. Furthermore, the sutureless adhesive sealing of the sockets physically by bioadhesive can achieve blood-coagulation-independent hemostasis and reduce the risk of bacterial infection, which is particularly crucial in emergency clinical settings [33–36]. However, commercially available injectable bioadhesives (e.g., fibrin glue, cyanoacrylates, and albumin-based BioGlue) often suffer from limitations such as weak and/or slow adhesion on wet tissues, poor mechanical properties, and potential immunogenicity [4, 37–39]. These shortcomings underscore the unmet clinical needs and the importance of developing new bioadhesives for effective socket wound care.

Numerous studies have shown that the formation of blood clots within the socket after extraction is a fundamental step in wound healing [40,41]. These clots not only stop bleeding but also serve as a provisional matrix to protect the denuded tissues and support cell migration [42,43]. Moreover, the autologous blood clots can also initiate and regulate the local immune microenvironment and release growth factors for the following well-orchestrated physiological process of bone healing [44,45]. Therefore, it is of significant importance to maintain the stability of post-extraction blood clots during the early-stage healing period in dental health care.

Here, we describe an injectable and biocompatible hydrogel as a sutureless and coagulation-independent bioadhesive for treating post-extraction bleeding and alveolar bone resorption (Scheme 1). The hydrogel (Tetra-PEG) is composed of two US Food and Drug Administration-approved components: tetra-armed poly(ethylene glycol) succinimidyl succinate (Tetra-PEG-SS) and tetra-armed poly (ethylene glycol) amine (Tetra-PEG-NH$_2$). When injected into the deep and bleeding extraction socket, the fast ammonolysis reaction between Tetra-PEG-SS and Tetra-PEG-NH$_2$ ensures rapid *in situ* hydrogel formation. Meanwhile, robust wet tissue adhesion is formed through the covalent bonding between NHS groups and tissue amines [3,36]. Furthermore, the highly uniform network structure of Tetra-PEG hydrogel enables strong mechanical strength to protect the wound from various irritants [46]. In addition, the rapid biodegradation of the designed Tetra-PEG hydrogel is able to mitigate the inflammatory response and provide space for new tissue formation [36]. Based on these fascinating features, the engineered Tetra-PEG hydrogel can offer rapid and robust adhesive sealing of the extraction socket, potentially
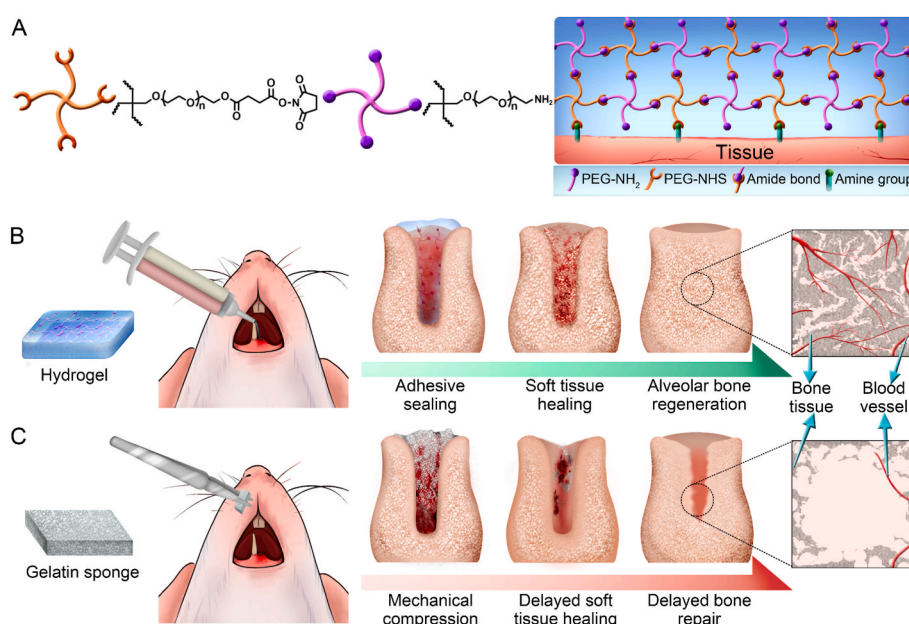


**Scheme 1.** Schematic illustration of the Tetra-PEG hydrogel bioadhesive for post-extraction hemostasis and alveolar bone regeneration. (A) Chemical structures of the Tetra-PEG hydrogel and a schematic diagram illustrating the adhesive interface formed through covalent amide bond cross-linking. (B) The rapid and robust adhesive sealing of the socket wound through *in situ* gelation of the injectable Tetra-PEG hydrogel can effectively halt post-extraction bleeding and stabilize the blood clots for tissue healing and bone regeneration. (C) In comparison, the filled gelatin sponge fails to provide durable and effective protection for the socket wound, resulting in partial loss of the blood clots, delayed wound healing, and poor bone formation.

addressing key limitations of sutures and commercially available dressings. We systematically characterized the gelation, mechanical strength, swelling ratio, tissue adhesive, and blood clot stabilization properties of the Tetra-PEG hydrogel. The coagulation-independent hemostatic ability and soft tissue wound healing effect of the hydrogel were evaluated in a heparinized rat anterior tooth extraction model, compared to the clinically used cotton and gelatin sponge. We further investigated the alveolar ridge preservation and *in situ* alveolar bone regeneration by this hydrogel through micro-CT and histomorphological analyses *in vivo*.

## 2. Materials and methods

### 2.1. Materials

Hydroxy-terminated tetra-arm poly(ethylene glycol) (Tetra-PEG-OH, $M_w = 10$ kDa) and tetra-arm poly(ethylene glycol)-amine (Tetra-PEG-NH$_2$, $M_w = 10$ kDa) were purchased from Sinopeg Biotech Co., Ltd. (Xiamen, China). Artificial saliva (AS, pH 7.4) was obtained from Coolaber (Beijing, China). Succinic anhydride, *N*-(3-dimethylamino-propyl)-*N′*-ethylcarbodiimide hydrochloride (EDC) and *N*-hydroxysuccinimide (NHS) were obtained from Energy Chemical, China. The fresh porcine tissues (skin, jaw, and palatal mucosa) were purchased directly from a local market. Tetra-armed poly(ethylene glycol) succinimidyl succinate (Tetra-PEG-SS) was prepared according to our previous reports [36], and the experimental details were provided in the Supporting Information.

### 2.2. Instrumentations

$^1$H NMR spectra were analyzed on a Bruker AVIII HD 400 MHz NMR spectrometer (Bruker, Germany), and FT-IR spectra were collected using KBr pellets on a Nicolet Magna IR-750 FT-IR spectrometer (Nicolet, USA) at room temperature. Scanning electron microscope (SEM) images of the samples were captured using a Hitachi Regulus 8100 (Japan) at 20 kV.

### 2.3. Hydrogel preparation

Tetra-PEG-NH$_2$ and Tetra-PEG-SS were individually dissolved into PBS solution (pH 7.4) with a designed final concentration of 10 *wt*%, 15 *wt*%, and 20 *wt*%, respectively. Subsequently, the Tetra-PEG hydrogel was prepared by mixing the two solutions with equal volume using a dual syringe.

### 2.4. Gelation time test

Since the hydrogel was applied to the bleeding site that was full of blood, the gelation time of the Tetra-PEG hydrogel was evaluated by injection of the precursor solution (10 *wt*%, 15 *wt*%, and 20 *wt*%) into an equal volume of citrated porcine whole blood. The gelation time was defined as the time when no liquid flowed upon inverting the vial. Each experiment was repeated three times.

### 2.5. Swelling ratio test

Cylindrical hydrogels (20 mm in diameter and 3 mm in height) (initial wet weight measured as $W_0$) were immersed in 10 mL of deionized water, artificial saliva, and anticoagulated porcine blood at 37 °C, respectively (n = 5 per sample). The hydrogels were taken out at specific time intervals, and the surface water was removed with filter paper and weighted as $W_s$. The swelling ratio (SR) was calculated as SR (%) = $(W_s - W_0)/W_0 \times 100$%.

### 2.6. Compression test

The compression performances of the pristine hydrogels and the hydrogels at swelling equilibrium state in deionized water, artificial saliva, and anticoagulated porcine blood were performed using a universal tensile machine (ETN503A WANCE, China) at a strain rate of 5.0 mm/min (n = 3 per sample) until hydrogel fracture or the compressive strain reached 90%. The precise dimensions of each hydrogel were measured using a digital caliper.

### 2.7. Adhesive strength

To assess the adhesive strength, Tetra-PEG-NH$_2$ and Tetra-PEG-SS precursor solutions were separately applied to the end surface of two different porcine skins (rectangle sizes of 50 mm × 15 mm) with an area of 15 × 15 mm evenly. Then, the two porcine skins coated with polymer solution were attached and placed under a 500 g weight for 30 s. The lap-shear adhesive strength of the sample was measured using a universal tensile machine (ETN503A WANCE, China) at a strain rate of 5.0 mm/min (n = 3 per sample). The adhesive strength of the attached samples after reaching equilibrium in deionized water, anticoagulated porcine whole blood, and artificial saliva was also tested.

Torsion assay was also employed to evaluate the adhesive stability of the Tetra-PEG hydrogel to the porcine mucosal tissue. The Tetra-PEG hydrogel was administered onto the tissue surface using a dual syringe. Then, the bending and twisting deformations were applied to the tissues, and the torsional pictures were captured. The adhesive interfaces between the Tetra-PEG hydrogel and the rat tissues (gingiva and alveolar bone) were examined using scanning electron microscopy (SEM) and hematoxylin and eosin (H&E) staining.

### 2.8. In vitro sealing stability

The premolar teeth of the porcine jaw were extracted, and the extraction sockets were rinsed extensively with PBS. Afterward, the citrated porcine whole blood was injected into the extraction sockets, followed by sealing with the Tetra-PEG hydrogel or gelatin sponge. The untreated extraction socket was tested as a control. The sealed porcine jaw was then immersed in a PBS buffer containing a large amount of dispersed rat food. The shear forces were induced by stirring, mimicking the dynamic environment in the oral cavity. Photographs of the extraction sockets were taken to monitor the sealing stability. In addition, the stabilization of blood clots was also evaluated by the method described above using recalcified citrated blood, and the sealed porcine jaw was transferred into the rat food desperation solution after 10 min of blood clotting. The extraction socket filled with recalcified citrated blood was taken as control.

### 2.9. In vitro degradability

The cylindrical Tetra-PEG hydrogels (10 mm diameter and 5 mm height) after lyophilization were weighted ($W_d$) and then submerged in artificial saliva or anticoagulated porcine blood in a shaking incubator at 37 °C (n = 5 per sample), respectively. The hydrogel samples were weighed ($W_t$) at specific intervals after lyophilization. The degradation behavior of hydrogel was characterized as the mass remaining (%), which was calculated as mass remaining (%) = $W_t/W_d \times 100$%.

### 2.10. Cell viability

1.0 g of Tetra-PEG hydrogel was first immersed into the Dulbecco's modification of Eagle's medium (DMEM) supplemented with 10% fetal bovine serum (FBS) and 1% penicillin/streptomycin (10 mL) for 24 h to obtain the hydrogel leachate. The human gingival fibroblasts (HGFs) (Procell, China) and rat bone marrow stem cells (BMSCs) (Procell, China) were seeded at 2000 cells/well on 96-well plates. After 24 h of

incubation at 37 °C in 5% $CO_2$, the cells were treated with hydrogel leachate and incubated for different times (1, 2, and 3 days). The cells treated with normal culture media were used as the control. The cell viability was assessed using the CCK-8 assay by measuring the absorbance at 450 nm using a microplate reader (n = 5). Besides, the cells were stained with a LIVE/DEAD Viability/Cytotoxicity Kit to visualize the cell morphology by a Leica DMi8 inverted fluorescence microscope (Leica Microsystems CMS GmbH, Germany).

### 2.11. Anterior tooth extraction in rat model

The animals were obtained from Vital River Laboratory Animal Technology Co., Ltd. (Beijing, China), and all animal studies on rats were conducted in strict adherence to the protocols approved by the ethical committee of Southern University of Science and Technology (Protocol No. SUSTech-JY202109009). Before commencing the experiment, Sprague-Dawley (SD) rats (8 weeks old, weighing 250–300 g) were allowed to acclimatize for one week. In this study, the rats were randomly allocated to three groups (n = 12 per group). An intraperitoneal injection of 2% pentobarbital sodium (at a dose of 50 mg/kg) was administered for anesthesia. Penicillin (80000 U) was given after anesthesia via intramuscular injection to prevent infection.

After anesthesia, the SD rat naturally opened its mouth and exposed the mandibular anterior teeth. A homemade rat gingival separator was first used to separate the gingival tissue, with a slight rotation of the gingival separator was used to facilitate teeth loosening and prevent damage to the surrounding soft tissue during tooth extraction. Subsequently, an intraperitoneal injection of heparin solution (2500 U/kg) was performed, and the rat was then positioned on a table with the limbs fixed using thick ropes. After a 10-min wait for the heparin to take effect, the anterior tooth was clamped with dental forceps, and the beak of the forceps was aligned with the long axis of the teeth. At this point, the rat's neck was tilted backward slightly, and gauze was placed under the head to protect the cervical spine. Then, the tooth extraction forceps were carefully manipulated to release the teeth. The surgery operation needed to be halted as there was a noticeable sensation of anterior tooth detachment. The rat was lying on its side to prevent the entrance of blood into the trachea after tooth removal. Finally, the entire anterior tooth was extracted slowly. The same tooth extraction procedure was also applied to the normal rats, except for the injection of heparin.

### 2.12. Hemostatic efficiency

After successfully establishing the anterior tooth extraction model in SD rats with or without heparin, the bleeding wound was immediately treated with Tetra-PEG hydrogel that formed *in situ*. The wounds treated with cotton ball (CO) by continuous manual pressure and the wounds filled with gelatin sponge (GS) were used as control groups. The blood loss in each group was collected using a pre-weighted cotton roll and measured as the weight change of the cotton roll before and after blood absorption. The time to hemostasis was also recorded for each group. The sealed wounds were monitored for another 3 min to ensure complete hemostasis.

### 2.13. Soft tissue healing

To evaluate the healing progress of the soft tissue, the extraction area of each rat was observed daily using a camera. The wound area was analyzed using ImageJ software (version: 1.52n).

### 2.14. Micro-CT analysis

The bone morphology within the tooth extraction socket at days 0 and 28 was analyzed by *in vivo* micro-CT (SkyScan 1276, Bruker, Belgium) operated at 100 kV and 200 μA. The SD rats were anesthetized with 2% isoflurane and securely positioned on the micro-CT scanning

table. A 180-degree rotation scanning was performed. The acquired raw images were reconstructed using the NRecon software (version: 1.7.1.6) using the same parameters for all rats. CTvox software (version: 3.3), a 3D visualization software, was employed to visualize the bone formation within the tooth extraction socket.

To evaluate the alveolar ridge height and width variations, the bilateral mandibles of the rats were carefully separated without damaging the mandibular midline joint after euthanasia by $CO_2$ inhalation on day 28 after surgery. The explanted bilateral mandibles were fixed with 4% paraformaldehyde solution into 50 mL centrifuge tubes for 48 h. Then, the centrifuge tubes were securely fixed to the sample table, and a 180-degree rotation scan was conducted (100 kV, 200 μA). NRecon, CTvox, and ImageJ software were used to analyze the changes in alveolar ridge height and width.

To further evaluate the *in vivo* osteogenesis, the mandible was isolated at days 7 and 28 and fixed with 4% paraformaldehyde solution. Each specimen was scanned using 180-degree rotation at 100 kV and 200 μA. The original scanned images were reconstructed using NRecon software. Dataviewer (version: 1.5.4.6) and ImageJ software were used for the image analysis of bone formation in the sagittal and coronal planes. Bone density (BMD) and bone volume/total volume (BV/TV) in the defect area were quantitatively analyzed from the micro-CT images. CTAn software (version: 1.17.7.2) was used to reconstruct the region of interest, and the bone quality was observed using CTvox software.

### 2.15. In vivo blood and organ toxicity analysis

On the 28th day after tooth extraction, 4 mL of blood was taken from each rat by cardiac puncture for blood analysis (complete blood count and blood chemistry analysis). Meanwhile, the heart, liver, spleen, lung, and kidney samples of the hydrogel group were collected and stained with H&E. The sections were studied using the Pathology slide scanner (NanoZoomer S60, Japan).

### 2.16. Histology and immunohistochemical (IHC) analysis

After dehydration, the fixed tissue samples were embedded into the paraffin and then cut into sections of a thickness of 5 μm for histological analysis, including H&E, Masson's trichrome, and Movat's pentachrome staining. Histological assessment was performed by two experienced pathologists, and the representative histological images of each group were listed.

For immunohistochemical studies, sections (thickness: 5 μm) were deparaffinized, dehydrated using anhydrous ethanol and washed with deionized water. Subsequently, the antigen repair was performed using citrate acid buffer (pH 6.0). To block endogenous peroxidase in the tissue, the sections were immersed in 3 $wt$% $H_2O_2$ solution and placed at room temperature for 30 min. After blocking the nonspecific binding sites with 3 $wt$% BSA/PBS solution at room temperature for 30 min, the sections were incubated overnight at 4 °C with primary antibody (CD31, 1:100). The sections were washed with PBS (pH 7.4) and covered with secondary antibody (goat anti-rabbit IgG (H + L), 1:200) followed by incubation at room temperature for 50 min. The sections were then stained with 3-diaminobenzidine, and the nuclei were stained with hematoxylin for about 3 min, then rinsed with water, and finally dehydrated and sealed. Immunohistochemical staining images were observed using the Pathology slide scanner (NanoZoomer S60, Japan). For further quantitative analysis, the percentage of the positive area was analyzed using ImageJ.

### 2.17. Statistical analysis

All the data were processed with GraphPad Prism 9.1.0 and presented as the mean ± S.D. One-way analysis of variance (ANOVA) was used to determine the significance level between multiple groups, and the significance level was considered as *$p < 0.05$, **$p < 0.01$, ***$p <$

0.001, ****$p < 0.0001$, and not significant (*ns*) with $p > 0.05$.

## 3. Results and discussion

### 3.1. Synthesis and characterization of the Tetra-PEG hydrogel

Tetra-PEG-SS was synthesized by activating the terminal carboxyl groups on tetra-armed poly(ethylene glycol) succinic acid with *N*-hydroxysuccinimide. As shown in Fig. S1, all the protons were well assigned in the $^1$H NMR spectrum, and the integration ratio of the NHS protons ($I_h$) to the methylene protons of the PEG chain adjacent to the ester group ($I_e$) was close to 2.0, suggesting the successful synthesis of Tetra-PEG-SS. FT-IR spectrum of Tetra-PEG-SS also revealed the characteristic absorption bands of ester and ether groups at 1735 and 1105 cm$^{-1}$, respectively. The Tetra-PEG hydrogel was then formed by rapidly mixing equal volumes of Tetra-PEG-SS and Tetra-PEG-NH$_2$ precursor solutions in PBS using a double-barrel syringe (Fig. 1A). A static mixer with a curved tip was connected to the cylinder syringe to facilitate homogeneous mixing and allow injection into various extraction sites, including the narrow, deep, and complex ones. A suitable gelation time was critical for rapid and efficient hemostatic sealing of the extraction socket while allowing smooth injection. The gelation time of Tetra-PEG hydrogel at varying solid contents was characterized by performing the vial tilting tests after injecting precursor solution into the same volume of anticoagulated porcine blood. As shown in Fig. 1B and C, the gelation time decreased significantly from 139 s to 81 s and 40 s as the solid content increased from 10 *wt*% to 15 *wt*% and 20 *wt*%, respectively. However, a further increase in solid content to 25 *wt*% resulted in needle clogging during injection (Fig. S2). Therefore, the hydrogel made of 20 *wt*% precursor solution was chosen for further studies.

The porous structure and proper swelling behavior of hydrogel play a major role in hemostatic sealing and tissue regeneration, owing to their contributions to absorbing the blood and excessive exudates, facilitating the exchange of gas and nutrients, and maintaining a moist healing environment [47–49]. SEM images revealed the porous structure of the lyophilized hydrogel due to the sublimation of ice crystals (Fig. 1D). We further compared the swelling properties of the Tetra-PEG hydrogel in deionized (DI) water, artificial saliva (AS), and anticoagulated whole blood (AB) (Fig. 1E and F). The hydrogel absorbed the liquid quickly within the first 4 h, and the swelling ratios reached the maximum values of $267.8 \pm 30.0\%$, $246 \pm 22.4\%$, and $145 \pm 31.1\%$ after soaking into DI water, AS, and AB for 12 h, respectively. Excessive swelling can be detrimental to the mechanical and adhesive properties and cause severe complications such as cord and nerve compression [3,38]. Notably, these values were lower than the swelling ratios of the other PEG-based sealants (up to 400%) [50] due to the highly homogeneous network of the Tetra-PEG gel, thus reducing the risk of tissue compression.

The hydrogel used for extraction socket sealing should have sufficient mechanical strength to retain the structural and functional integrity under external forces such as chewing, licking, swallowing, and talking behaviors. The compressive strength of Tetra-PEG hydrogel before and after soaking in DI water, AS, and AB were studied (Fig. 1G and Fig. S3). The pristine gel demonstrated a compressive stress of around 5400 kPa at 90% strain. After swelling equilibrium was established, the swollen Tetra-PEG gel remained mechanically strong with a compressive strength ranging from 380 kPa to 880 kPa. Furthermore, we assessed the *in vitro* degradation of the Tetra-PEG hydrogel through incubation in artificial saliva and anticoagulated blood (Fig. 1H). The hydrogel displayed a slow degradation pattern, with only about 8% weight loss observed within the first two days. Afterward, the Tetra-PEG hydrogel degraded quickly and dissolved completely within three days, originating from the faster cyclization degradation of the unique
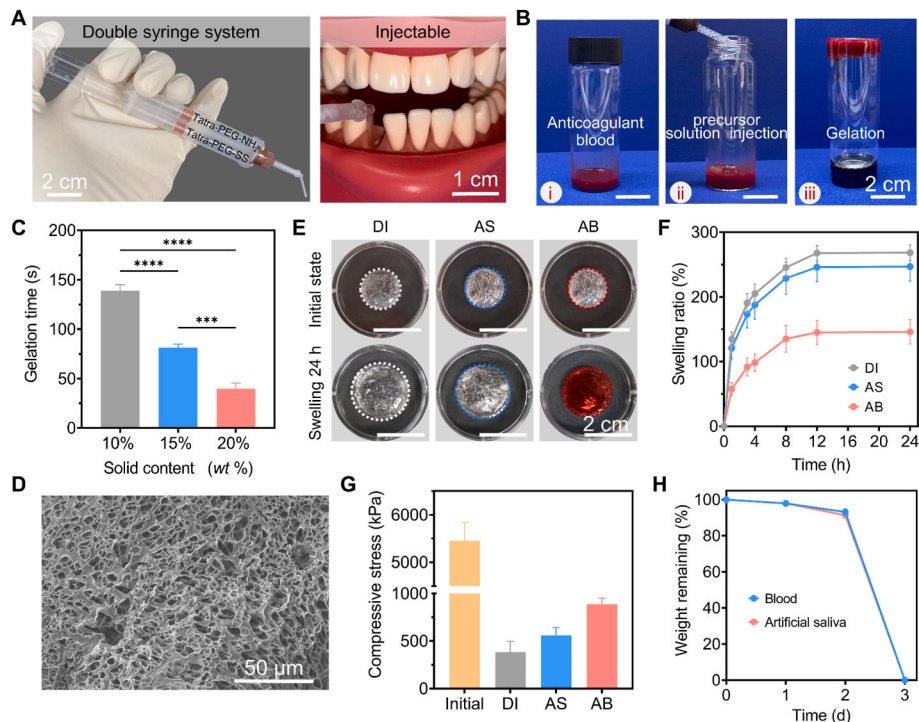


**Fig. 1.** Preparation and characterization of the Tetra-PEG hydrogel. (A) Photographs of the cylinder syringe with a curved tip that allows convenient injection into the deep tooth sockets. (B) Photographs of the gelation time testing by injecting the precursor solutions into an equal volume of anticoagulated blood. Taking 20 *wt*% solid content as an example (scale bar: 2 cm). (C) The average gelation time of the hydrogels with various solid contents (n = 3). (D) Representative SEM image of the Tetra-PEG hydrogel prepared with 20 *wt*% solid content (scale bar: 50 μm). (E, F) Photographs (E) and the average swelling ratios (F) of the hydrogels after being immersed in deionized water, artificial saliva, and anticoagulated porcine whole blood (n = 5, scale bar: 2 cm). (G) Compressive stress of the Tetra-PEG hydrogels before and after reaching swelling equilibrium (n = 3). (H) The weight remaining of the hydrogel in anticoagulated porcine whole blood and artificial saliva, respectively (n = 5). Error bars are small and not visible. All data are presented as mean ± S.D. (***$p < 0.001$ and ****$p < 0.0001$).

succinyl ester groups [36].

### 3.2. Tissue adhesive of Tetra-PEG hydrogel

An ideal intraoral hydrogel sealant should also have high tissue adhesion to anchor firmly to the wet tissue, maintain hemostatic sealing, and protect the wound from the external environment. A torsion test was first performed to determine the adhesive ability of Tetra-PEG hydrogel on soft tissue. Due to the difficulties in obtaining a larger area of gingival tissue, fresh and wet porcine palatal mucosa was used as a biological substrate. As shown in Fig. 2A, the *in situ* formed hydrogel adhered tightly to the palatal mucosa surface without any sign of peeling off and retained its intact structure under bending and twisting stresses, demonstrating the flexibility of Tetra-PEG hydrogel and the formation of strong interface bonding. A lap shear test was further conducted to quantitatively determine the shear strength of the hydrogel (Fig. 2B and Fig. S4). The newly formed Tetra-PEG hydrogel adhered to the pigskin and showed a shear strength of 30.3 ± 2.5 kPa. When the sample reached its fully swollen state, the shear strength dropped to ~12.4–18.9 kPa due to the decreased mechanical properties of the hydrogel, as discussed above. Nonetheless, the fully swollen Tetra-PEG hydrogel still exhibited a higher adhesive performance than fibrin glue (~3.9 kPa), one of the most extensively used clinical tissue adhesives (Fig. S5).

The microstructure of the adhesion interface was further examined by SEM and H&E staining [51,52]. The Tetra-PEG hydrogel was deposited *in situ* to the rat gingiva and alveolar bone tissues. SEM and histologic images revealed a tight adhesion between the hydrogel and the gingival tissue (Fig. 2C and D). Additionally, the entanglements observed through SEM imaging between the hydrogel and collagen fibers indicated that the free PEG chains infiltrated the tissue matrix during sol-gel transition, resulting in mechanical interlocking with the gingiva tissue [4,53]. Similarly, a tight and conformal interface adhesion was presented between the hydrogel and rat alveolar bone. Thus, the physical interlocking and the chemical reaction between the residual NHS groups and underlying tissue amines synergistic contributed to the favorable adhesive performance of the Tetra-PEG hydrogel.

To demonstrate the sealing stability of the hydrogel, an *in vitro* porcine jaw model was built to mimic the dynamic mechanical environments (e.g., eating, drinking, and licking) in the oral cavity. Anticoagulated porcine blood was first injected into the extraction socket, followed by sealing with the *in situ* forming Tetra-PEG hydrogel or GS (Fig. 2E). The porcine jaw was then immersed in PBS containing rat food, and the solution was vigorously stirred to induce shear forces. After soaking for 5 min, a large number of food granules entered the untreated extraction socket. It was found that the GS was broken within 3 h, and the food granules occurred into the extraction socket. After 48 h of continuous stirring, the socket in the GS group was filled with food
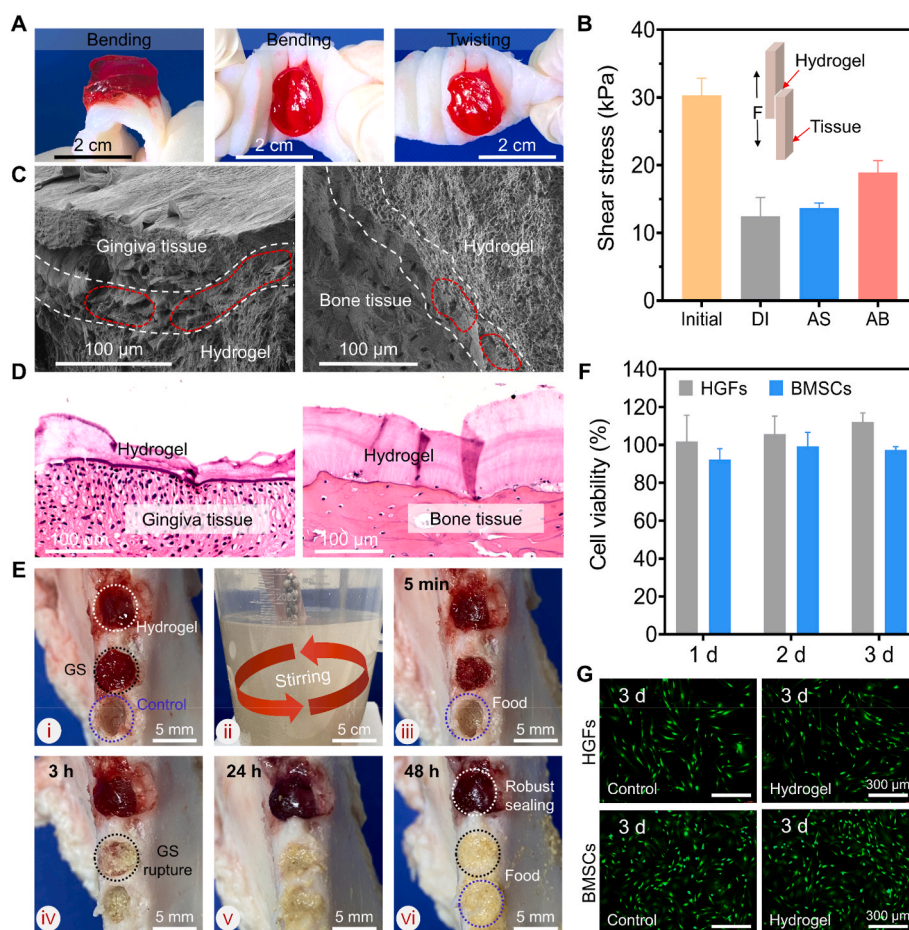


**Fig. 2.** The *in vitro* adhesive properties and biocompatibility of the Tetra-PEG hydrogel. (A) Photographs of the *in situ* formation hydrogel onto the porcine mucosal tissue that suffers from different deformations (scale bar: 2 cm). (B) Lap shear strength of the Tetra-PEG hydrogel in its initial state and after equilibrium swelling in DI water, AS, and AB, respectively (n = 3). (C, D) The representative SEM (C) and H&E-stained (D) images of the adhesion interfaces between the rat tissues (gingiva and alveolar bone) and hydrogel (scale bar: 100 μm). In SEM images, the white dotted area represents the fractured hydrogel-tissue interface, and the red circle indicates the remaining entanglements after freeze-fractured. (E) Comparison of the *in vitro* sealing abilities of the Tetra-PEG hydrogel and gelatin sponge using a porcine jaw filled with anticoagulated blood. (F, G) Cell viability (F) and LIVE/DEAD assay images (G) of HGFs and BMSCs against the hydrogel, respectively (n = 5, scale bar: 300 μm). All data are presented as the mean ± S.D.

granules comparable to that of the untreated one, indicating sealing failure. In contrast, the hydrogel could withstand the external stresses with no obvious morphology change and keep the defect from food debris throughout the observation period up to 48 h. We further evaluated the sealing stability of the blood clots using recalcified whole blood. As shown in Fig. S6, the newly formed blood clots in the control group detached within just 5 min. The GS ruptured and the food granules accumulated within the socket after 3 h. Again, our hydrogel adhesion remained robust after a 48-h observation period. These findings suggested that our Tetra-PEG hydrogel could provide a fluid-tight sutureless sealing and effectively protect the blood clots within the extraction socket.

### 3.3. In vitro biocompatibility

Biologically compatible is the prerequisite for the clinical application of adhesives. HGFs and BMSCs were selected to evaluate the *in vitro* biocompatibility of the Tetra-PEG hydrogel, owing to their essential role in wound healing and bone regeneration [54,55]. The cells were co-cultured with the hydrogel extract for three days. The cell viability of hydrogel tested by CCK-8 assay was higher than 90% for both cell types

(Fig. 2F). Additionally, LIVE/DEAD cell staining showed normal morphologies and nearly undetectable red fluorescence (dead cells), comparable to the control group (Fig. 2G and Fig. S7). These results confirmed the high biocompatibility of Tetra-PEG hydrogel for potential oral applications.

### 3.4. Rapid and coagulation-independent hemostatic sealing

An anterior tooth extraction model was created on the healthy and anticoagulant-treated SD rats (Fig. 3A). To evaluate the hemostatic sealing efficacy of Tetra-PEG hydrogel qualitatively, we performed an *in vivo* hemostatic assay by measuring the blood loss and time to hemostasis (Fig. 3B–E). CO and GS were used as the control groups. Immediately after the surgery, the CO was applied to the wound site with continuous manual pressure while the GS was directly inserted into the bleeding cavity. Fig. 3B showed the hemostatic process in normal rats after tooth extraction. As shown in Fig. 3D and E, the CO group could stop the bleeding with an average blood loss of 370 mg and hemostatic time of 307 s. For the GS group, the accumulated blood loss and time to hemostasis were reduced to 188 mg and 116 s, respectively. Impressively, the hydrogel group achieved efficient hemorrhage control with
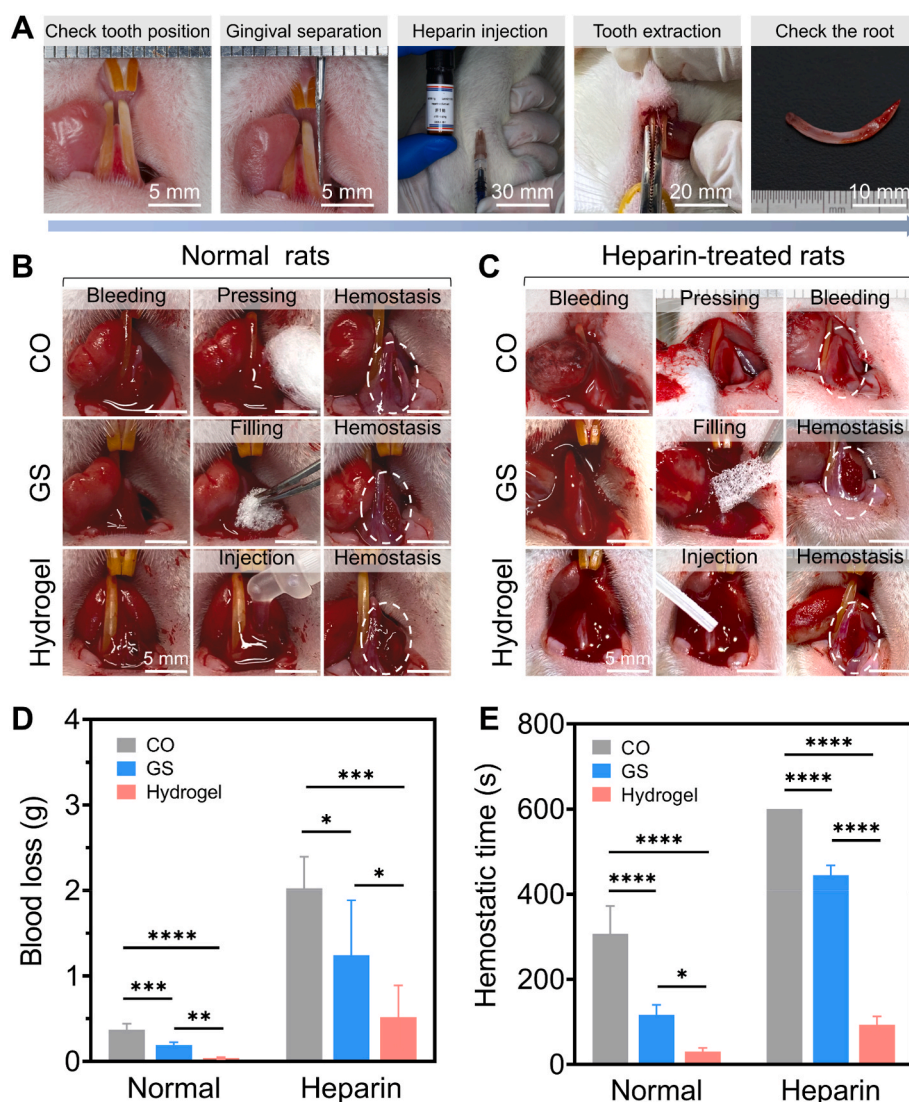


**Fig. 3.** *In vivo* hemostatic efficacy of the Tetra-PEG hydrogel in a rat anterior tooth extraction model. (A) Representative photographs for the establishment of a heparinized rat anterior tooth extraction model. (B, C) Experimental images of the bleeding after tooth extraction and the hemostatic process using Tetra-PEG hydrogel, cotton, and gelatin sponge in (B) normal and (C) heparinized rats, respectively. (D, E) Summary of the blood loss and hemostatic time of each sample in the rat anterior tooth extraction model (n = 6). All data are presented as the mean ± S.D. (*$p < 0.05$, **$p < 0.01$, ***$p < 0.001$, ****$p < 0.0001$).

remarkably reduced blood loss (38 mg) and hemostasis time (30 s) compared to the CO and GS groups.

To further assess the hydrogel's hemostatic capabilities in a more challenging scenario, we employed a heparinized rat tooth extraction model, mimicking anticoagulated patients (Fig. 3C). It was found that the CO group failed to cease bleeding with the application of manual pressure for over 10 min, as demonstrated by the occurrence of apparent blood leakage. In addition, the GS-treated group took more than 7 min to accomplish hemostasis with a total blood loss of 1246 mg. By comparison, our Tetra-PEG hydrogel was capable of halting the post-extraction hemorrhage under anticoagulated condition with ~80% and ~60% reduction in hemostatic time and blood loss compared to the GS group, respectively.

The hemostatic results described above proved the efficacy of our Tetra-PEG hydrogel in halting post-extraction bleeding, even under the anticoagulated condition, substantially outperforming the CO and GS groups. This remarkable hemostatic capability could be attributed to the fascinating features of Tetra-PEG hydrogel, including the *in situ* injectability, rapid gelation, instant and tough tissue adhesion, and high mechanical strength, which could rapidly form an adhesive hydrogel barrier to seal the wound sites tightly. These results collectively demonstrated the capacity of Tetra-PEG hydrogel to serve as an injectable and coagulation-independent hemostat for halting life-threatening hemorrhages after tooth extraction.

### 3.5. In vivo soft tissue wound healing

Having demonstrated the superior hemostatic sealing of Tetra-PEG hydrogel, we moved on to evaluate the soft tissue defect repair following tooth extraction in the heparinized rat (Fig. 4A). No stable blood clots were formed, and blood oozing was observed within the exposed extraction socket in the CO-treated animal on day 1, which was due to the coagulation disorder and continuous external disturbances within the oral cavity. By day 2, granulation tissue was present to fill the entrance of the socket in the CO group, but a large amount of the newly

formed granulation tissue fell off on the 4th day, which might induce dry socket (also known as alveolar osteitis) and severely delay wound healing. Over the follow-up period for the CO group, the granulation tissue was rebuilt within the socket, and the defect was gradually closed. The porous structure of the gelatin sponge could absorb and coagulate whole blood during hemostasis. Since the initially formed blood clots were brittle and easily disrupted, the weak mechanical strength of the sponge was unable to protect the wound from external irritations, thus resulting in partial loss of the blood clots on day 1. By the following week, the filled sponge underwent *in vivo* degradation, as indicated by the gradual decreases in size, accompanied by soft tissue healing. It should be noted that the GS detached on day 7, leaving a distinct unhealed area. As for the hydrogel-treated animals, the hydrogel bioadhesive could form a robust adhesion and anchor firmly to the soft tissue within the first three days. It can be observed that the Tetra-PEG hydrogel exhibited gradual biodegradation with an almost complete disappearance on day 4, showing a similar degradation profile to the above *in vitro* observation. As the entrapped blood clots were progressively replaced by granulation tissue, the extraction socket closed with an ignorable gap on day 8. Notably, the soft tissue repaired by the hydrogel yielded a smoother and more well-defined gingival contour, whereas the CO-treated defect without filler material healed with marked soft tissue collapse.

The wound closure area was further characterized to quantitatively evaluate the efficacy of Tetra-PEG hydrogel during the soft tissue healing process (Fig. 4B and C). The results in Fig. 4C showed that the average wound closure ratios were consistently increased for the three groups. By the 4th day of treatment, 42.3%, 40.0%, and 57.0% wound closure areas were obtained for the CO, GS, and hydrogel groups, respectively. The wound closure area of the hydrogel group increased to 80.9% on day 6, whereas the CO and GS-treated defects only healed with 57.3% and 56.1%, respectively. More importantly, we found that the extraction defect repaired by the hydrogel almost completely closed with wound closure area up to 99.5% after 8 days, significantly higher than both CO (83.0%) and GS (79.1%) groups. These findings revealed a
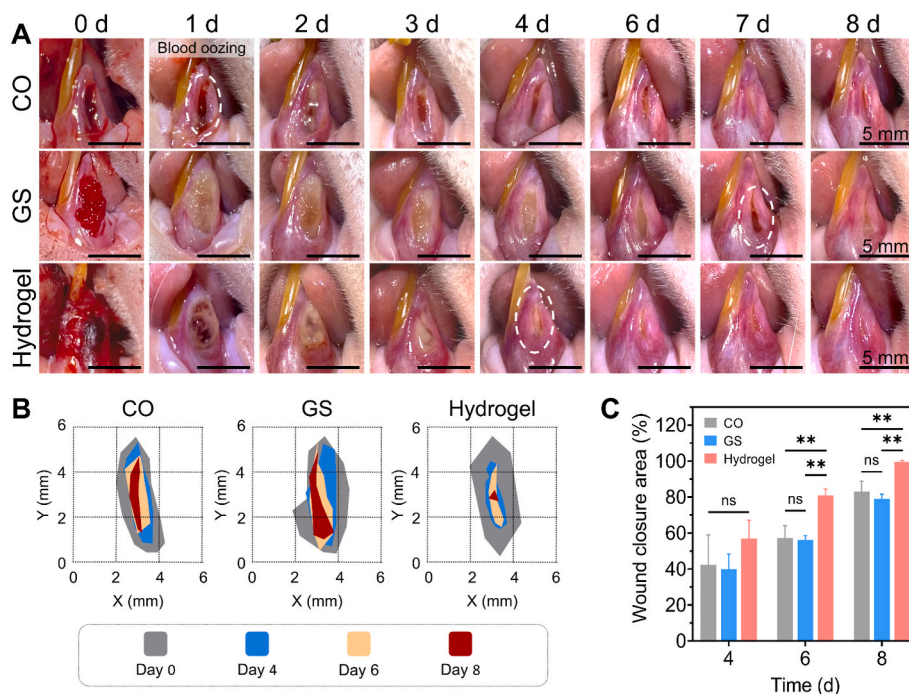


**Fig. 4.** *In vivo* soft tissue wound healing evaluation. (A) Representative photographs of the extraction wound treated with CO, GS, and Tetra-PEG hydrogel in a heparinized rat (scale bar: 5 mm). (B) Schematic diagram of the extraction wound contraction during the observation period of 8 days. (C) Wound closure area on days 4, 6, and 8 (n = 3). Quantification of wound closure area (%) was expressed as the percentage of the wound closed relative to the initial size (Day 0). The data are presented as the mean ± S.D. (**$p < 0.01$).

superior efficiency of Tetra-PEG hydrogel in promoting tooth extraction wound healing, which could be explained by the following several factors. The robust and stable adhesive sealing of the extraction socket by Tetra-PEG hydrogel in the early postoperative period served as an efficient barrier against complex irritations and was capable of protecting the blood clots and promoting tissue repair. Besides, the hydrogel can absorb excess exudate and maintain the wound bed moist to aid wound healing. Furthermore, the hydrogel degradation at the extraction site also provided space for the newly formed tissue to avoid impeding wound closure. By contrast, no statistically significant differences in wound healing were observed between the CO and GS-treated groups because of a relatively slow degradation rate of GS and partial loss of the blood clots.

### 3.6. Alveolar ridge preservation and in situ bone regeneration

Micro-CT scans were further performed to evaluate the bone regeneration after hemostasis, and the representative *in vivo* three-dimensional (3D) reconstruction micro-CT images were shown in Fig. 5A. The surgically created extraction socket displayed a hollow, smooth, and continuous bone surface without root fractures, suggesting the successful establishment of the anterior extraction model. Four weeks after tooth extraction, the newly formed bone tissue was observed

in each group to repair the alveolar bone defect. Notably, the socket treated with the hydrogel exhibited a smoother and denser alveolar bone surface compared to the CO and GS groups after 28 days.

To quantitatively assess the level of bone resorption, the relative dimensional changes in the alveolar ridge height and width at the lingual and labial sides as compared with the untreated adjacent tooth were measured. As shown in Fig. 5B and D, the average reduction in the lingual and labial heights of the hydrogel group was 3.9% and 6.1% at day 28, significantly lower than the CO and GS groups ($\sim$11.5% and $\sim$29.2% reduction, respectively). A similar trend with a lower change in the alveolar ridge width was also observed for the hydrogel group (Fig. 5C and E). These results demonstrated that the Tetra-PEG hydrogel could effectively reduce the morphologic alteration of the alveolar ridge and displayed superior alveolar ridge preservation compared to CO and GS after tooth extraction.

The representative micro-CT coronal and sagittal sections were shown in Fig. 6A and B, and the percentage of new bone area in the extraction socket was quantified (Fig. 6C and Fig. S8). By the seventh day after extraction, the average neo-bone area was determined to be 14.8% for the hydrogel group from the coronal plane view, 2.3-fold greater than that in the CO (4.7%) and GS (6.3%) groups. The percentage of the new bone area increased over time, and 53.0% was obtained for the Tetra-PEG group after four weeks. This value was also
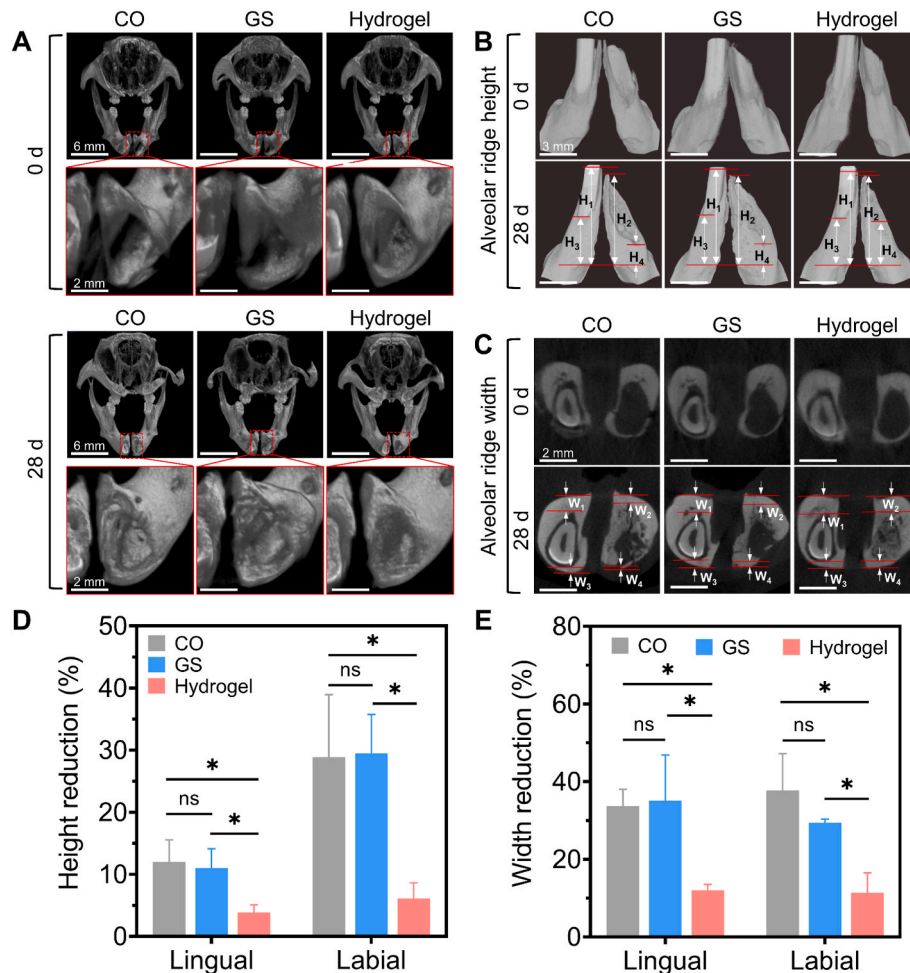


**Fig. 5.** Micro-CT analysis of the alveolar socket repair and alveolar ridge preservation. (A) Representative micro-CT images illustrating the alveolar socket immediately after tooth extraction (day 0) and the repaired alveolar socket after 28 days (top, scale bar: 6 mm). High-magnification views of the extraction site are presented (bottom, scale bar: 2 mm). (B, C) Changes in alveolar ridge height (B) and width (C) on day 28 (scale bars: 3 mm and 2 mm, respectively). Height reduction at the lingual and labial side was calculated as $(1\text{-}H_2/H_1) \times 100\%$ and $(1\text{-}H_4/H_3) \times 100\%$, respectively; Width reduction at the lingual and labial side was calculated as $1\text{-}(W_2/W_1) \times 100\%$ and $1\text{-}(W_4/W_3) \times 100\%$, respectively. (D, E) Quantification of the decreased alveolar ridge height (D) and width (E) for the lingual and labial regions (n = 3). The data are presented as the mean $\pm$ S.D. (*$p < 0.05$).
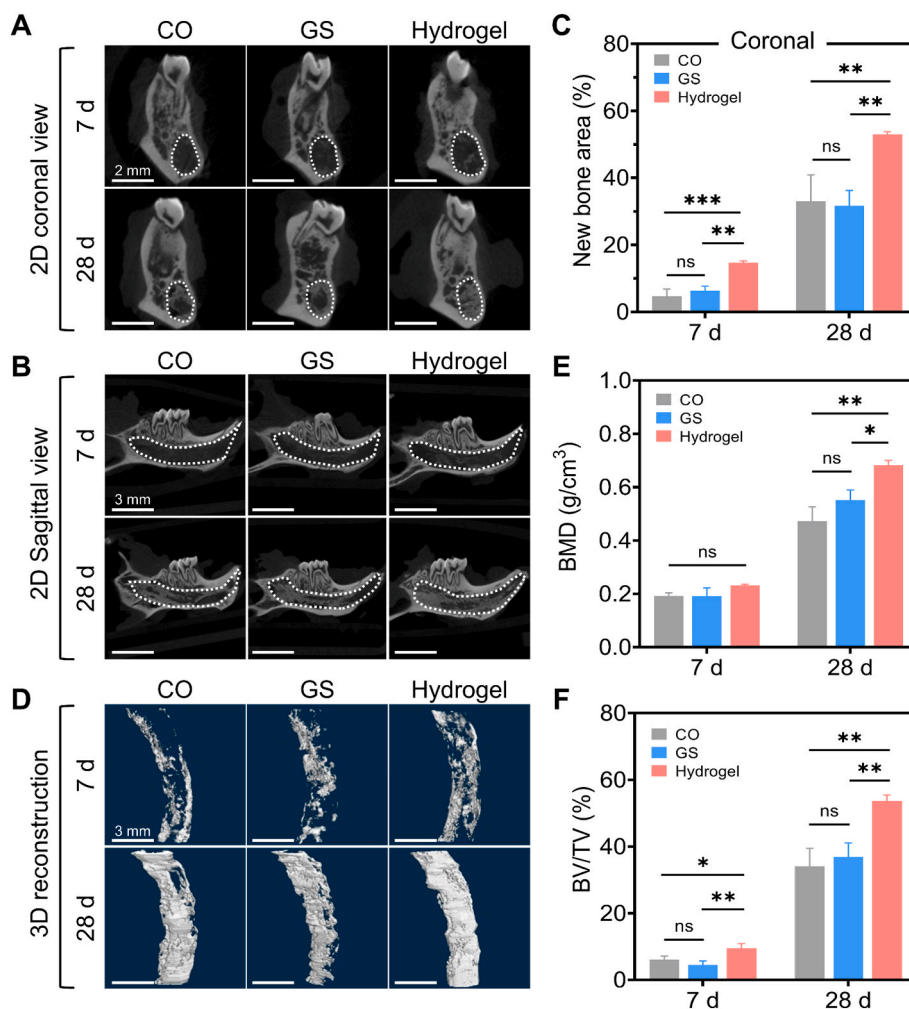
**Fig. 6.** *In situ* bone regeneration in a rat anterior tooth extraction model. (A, B) Representative coronal (A, scale bar: 2 mm) and sagittal (B, scale bar: 3 mm) sections of the rat anterior defect repaired by the CO, GS, and hydrogel on the 7th and 28th day after surgery. (C) Quantification of the relative percentage of new bone area in the extraction socket from the coronal images (n = 3). (D) 3D micro-CT reconstructions of the repaired bone defects at 7 and 28 days (scale bar: 3 mm). (E, F) Measurement of the BMD and BV/TV from 3D micro-CT reconstructions (n = 3). All data are presented as the mean ± S.D. (*$p < 0.05$, **$p < 0.01$, and ***$p < 0.001$).

much higher than those in the other two groups. Furthermore, the newly formed bone tissue in the CO and GS groups was mainly presented around the socket on day 28, with very little bone formation observed in the central region. In contrast, the Tetra-PEG hydrogel could induce a higher occupied area and more uniform distribution of the newly formed bone throughout the defect. Similarly, our Tetra-PEG adhesive also achieved a significant improvement in the new bone area (7.0% and 49.5%) compared to the CO (4.2% and 31.9%) and GS (4.9% and 33.7%) groups from the sagittal section on days 7 and 28, respectively (Fig. S8).

The 3D reconstruction images of the extraction socket revealed that a few new bone tissues formed and scattered in the defect area for all groups at 7 days. The hydrogel-treated defect consistently exhibited the highest level of bone regeneration, as evidenced by the significantly greater X-ray radiopacity (Fig. 6D). To further characterize the bone quality, histomorphometric parameters such as bone mineral density (BMD) and bone volume/total volume (BV/TV) were calculated. Higher BMD and BV/TV values indicated better bone quality regarding mechanical strength and volume fraction, respectively. As depicted in Fig. 6E and F, the Tetra-PEG hydrogel induced a greater BV/TV compared to the CO and GS groups after 7 days, but no significant differences were observed in the BMD. By day 28, the BV/TV and BMD increased in all groups, with the hydrogel group showing 1.4- and 1.5-fold higher values than the CO and GS groups, respectively. These findings suggested that the use of Tetra-PEG hydrogel as a tooth

extraction wound sealant could significantly enhance alveolar ridge preservation, promote *in situ* bone regeneration, and improve bone quality compared to CO and GS.

### 3.7. Histomorphological and immunohistochemical evaluation

Histological examinations, including H&E, Masson's trichrome, and Movat's pentachrome staining of the decalcified tissue sections, were further conducted to evaluate the process of bone formation within the extraction socket (Fig. 7). H&E staining provided an overall view of the bone morphology, microstructure, and inflammatory information. The bone tissue with a compact structure was stained with dark pink, and the blood clot consisted of red blood cells represented as red aggregates, while the connective tissue consisted primarily of collagen fibers and cells stained with light pink (Fig. 7A). Seven days after extraction, fibrous tissue was predominated in the CO group with apparent inflammatory cell infiltration, and the newly formed bone tissue with disconnected trabeculae mainly occurred in the marginal region. The GS group displayed a relatively large hole containing remnant blood clots on day 7, likely due to the detachment of the filled sponge. Surrounding the hole, connective tissue had occurred, and the newly formed bone was scattered near the alveolar wall, along with the invasion of some inflammatory cells. Notably, in the hydrogel group, the hydrogel was completely degraded after one week and a large amount of woven bone
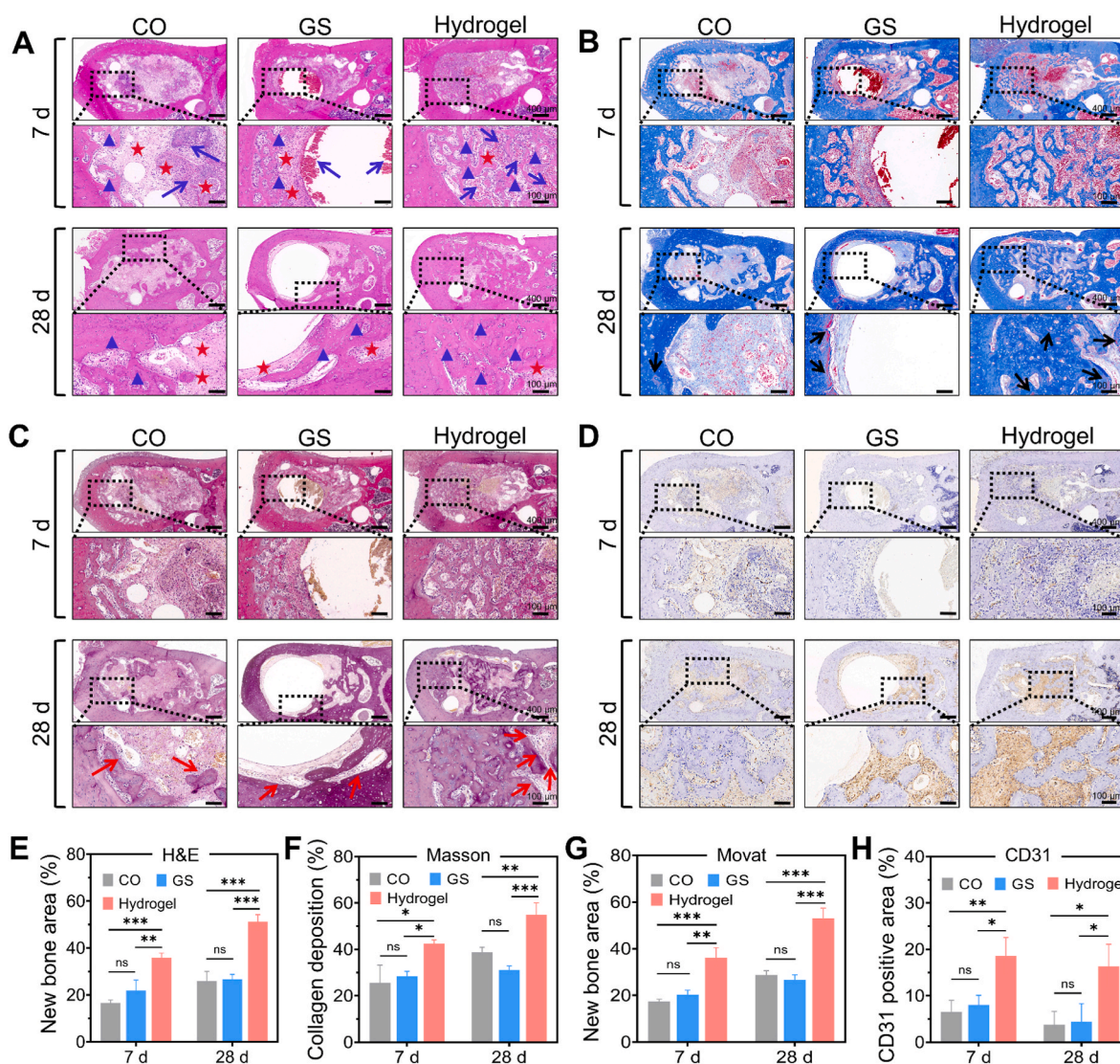
**Fig. 7.** Histomorphological and immunohistochemical analysis of socket healing and bone formation. (A–D) Representative H&E (A), Masson's trichrome (B), Movat's pentachrome (C) staining and immunostaining for CD31 (D) of the rat anterior extraction socket treated with CO, GS, and Tetra-PEG hydrogel after 7 and 28 days. A higher-magnification view is shown below. The blue triangle, red star, and blue arrows in H&E staining images indicate the presence of new bone area, fibrous tissue, and blood clots, respectively. In Masson staining images, the black arrows represent the mature bone. In Movat staining images, the red arrows represent the active osteoblasts (top, scale bar: 400 μm; bottom, scale bar: 100 μm). (E–H) Quantification of the relative new bone area (E and G, derived from H&E and Movat staining images, respectively.), collagen deposition (F), and CD31-positive capillaries (H) from the representative histological and immunohistochemical histomorphological images of the extraction socket treated with CO, GS, and Tetra-PEG hydrogel (n = 3). All data are presented as the mean ± S.D. (*$p < 0.05$, **$p < 0.01$, ***$p < 0.001$).

occurred to fill the extraction socket from the marginal region with compact and connected trabeculae, which radiated toward the center of the socket. Besides, residual blood clots were dispersed throughout the extraction socket, and no apparent inflammatory response was observed. After four weeks, all groups exhibited increased bone formation with almost no inflammatory response. The connective tissue primarily filled the socket with only a small number of bone islands observed in the marginal area in the CO group. In the GS group, the new bone formation was localized to the region around the hole. In contrast, most of the defect area in the hydrogel group was healed by sufficient new bone tissue. Further quantitative analysis showed a much higher new bone area percentage in the Tetra-PEG group than the others, consistent with the above micro-CT results (Fig. 7E).

Since collagen is the principal organic constituent of bone matrix, collagen deposition is a key factor in bone remodeling with a positive correlation to bone healing [56,57]. Masson staining was further performed to evaluate the collagen deposition and new bone formation

(Fig. 7B). After 7 days, both the CO and GS groups showed predominantly loose connective tissue and a small amount of strip-like new bone formation. Compared to the other two groups, the collagen fibers were more abundant in the hydrogel group, which extended from the wall toward the center of the socket. Besides, loose connective tissue was present, and primary trabeculae were aligned upon the collagen fibers to form a preliminary framework on which bone modeling proceeded. By day 28, dense fibrous connective tissue was formed in the CO and GS groups, and the bone trabeculae were found mainly concentrated in the marginal area with a limited number of matured ones. For the Tetra-PEG hydrogel group, the defect was healed with abundant thick, dense, and connected trabecular bone. The Haversian canals and blood vessels were detected in the newly formed bone tissue, and the collagen fibrils were organized in a helical pattern, demonstrating a regular bone formation in the hydrogel-treated socket. Notably, the presence of red staining confirmed mature bone formation. Quantitative analysis of the total collagen deposition indicated that more collagen was generated in the

hydrogel group during the observation period, confirming the positive effect of the Tetra-PEG hydrogel on bone healing (Fig. 7F).

Movat's pentachrome staining was further conducted to identify different tissue types. The results in Fig. 7C revealed the presence of abundant fibrous connective tissue and fewer newborn bone trabecula in the CO and GS groups on day 7. In contrast, the hydrogel group showed a higher level of bone trabecula formation, and substantial osteoblasts were located around the newly formed bone. Besides, the bone tissue was also surrounded by a layer of new osteoid that was not yet calcified. On day 28, the CO and GS groups displayed limited bone formation, mostly in the margins, with few osteoblasts or osteoid presented. However, the socket sealed by hydrogel was repaired with adequate new bone tissue that comprised a mixture of lamellar and woven bone. Bone formation was active in the hydrogel group, as demonstrated by the presence of osteoblasts in a cuboidal or fusiform shape, as well as the formation of small vessels. In addition, the quantitative analysis showed a significantly higher new bone formation in the hydrogel group compared to the CO and GS groups, consistent with the above H&E and Masson staining (Fig. 7G).

The new blood-vessel formation and establishment of the vascular network, which can supply oxygen, minerals, and nutrients necessary for mineralization, are crucial steps in bone healing [58,59]. We then evaluated the angiogenesis by immunohistochemical staining of CD31, a specific marker of endothelial cells, for further analysis. As shown in Fig. 7D and H, the hydrogel group displayed a remarkably higher expression level of CD31 with more vascularized connective tissue and increased microvessel density as compared to CO and GS groups one and four weeks after extraction, demonstrating the promotion of bone regeneration by hydrogel through enhancing new blood vessels formation. Furthermore, no signs of organ and systemic toxicity were found for the rats in the hydrogel group from the H&E staining and blood analyses four weeks after implantation (Fig. S9).

The histomorphological results revealed that Tetra-PEG hydrogel could effectively accelerate bone healing in extraction sockets with suppressed long-term inflammation, elevated collagen deposition, higher osteoblast activity, and enhanced angiogenesis compared to the CO and GS groups. These findings could be attributed to several factors. First, the injectable Tetra-PEG hydrogel could be filled into the deep socket and rapidly *in situ* self-gelation to achieve quick hemostatic sealing independent of blood condition while serving as a robust physical barrier to protect the socket from oral irritants, thus reducing the risk of postoperative complications. Second, the hydrogel absorbed blood and stabilized the blood clots in the extraction socket. The resultant hydrogel and hematoma complex were expected to act as a scaffold to support cell function and tissue growth, as well as offer a sustained release of growth factors and cytokines for bone repair during the initial healing stage. Moreover, the excellent biocompatibility and appropriate degradation behavior of the Tetra-PEG hydrogel could induce less inflammatory infiltration and result in more organized and completed bone formation. However, as for the anticoagulant bleeding defect treated by CO or GS, the blood clots failed to form promptly or were partially lost in the early period after tooth extraction, which ultimately resulted in significantly delayed wound healing.

## 4. Conclusions

In this article, we have described the use of an injectable Tetra-PEG hydrogel as a sutureless and anticoagulant-independent bioadhesive for the management of dental extraction, which was capable of achieving rapid gelation, firm tissue adhesion, high mechanical strength, appropriate degradability, and excellent biocompatibility. The rapid and robust adhesive sealing of the extraction socket by Tetra-PEG hydrogel could provide reliable protection for the defect while stabilizing the blood clots and supporting wound healing. The *in vivo* rat tooth extraction model with anticoagulation agent validated the efficacy of Tetra-PEG hydrogel in bleeding control, soft tissue wound closure,

alveolar ridge preservation, and *in situ* bone regeneration, superior to that of the widely used cotton and gelatin sponge. We further demonstrated that the Tetra-PEG hydrogel could accelerate bone healing through suppressed long-term inflammation, elevated collagen deposition, high osteoblast activity, and enhanced angiogenesis. Taken Together, this study highlighted the advantages of Tetra-PEG hydrogel, making it a promising injectable bioadhesive for post-extraction hemorrhage control and socket repair, particularly in patients receiving anticoagulant therapy.

## Ethics approval and consent to participate

This work does not contain results related to human participant.

All animal procedures were performed in accordance with the Guidelines for Care and Use of Laboratory Animals of the Southern University of Science and Technology and experiments were approved by the Animal Ethics Committee of the Laboratory Animal Center of Southern University of Science and Technology (Protocol No. SUSTech-JY202109009).

## CRediT authorship contribution statement

**Gang He:** Writing – original draft, Visualization, Methodology, Investigation. **Yiwen Xian:** Methodology, Investigation. **Huajun Lin:** Investigation. **Chengcheng Yu:** Investigation. **Luyuan Chen:** Investigation. **Zhihui Chen:** Investigation. **Yonglong Hong:** Supervision, Funding acquisition, Data curation, Conceptualization. **Chong Zhang:** Writing – review & editing, Supervision, Funding acquisition, Data curation, Conceptualization. **Decheng Wu:** Writing – review & editing, Supervision, Funding acquisition, Data curation, Conceptualization.

## Declaration of competing interest

Decheng Wu is an editorial board member for Bioactive Materials and was not involved in the editorial review or the decision to publish this article. All authors declare that there are no competing interests.

## Appendix A. Supplementary data

Supplementary data to this article can be found online at https://doi.org/10.1016/j.bioactmat.2024.03.015.

## References

[1] P.C. Passarelli, S. Pagnoni, G.B. Piccirillo, V. Desantis, M. Benegiamo, A. Liguori, R. Papa, P. Papi, G. Pompa, A. D'Addona, Reasons for tooth extractions and reapplated risk factors in adult patients: a cohort study, Int. J. Environ. Res. Public Health. 17 (7) (2020) 2575.

[2] K. Olcay, H. Ataoglu, S. Belli, Evaluation of related factors in the failure of endodontically treated teeth: a cross-sectional study, J. Endod. 44 (1) (2018) 38–45.

[3] S. Nam, D. Mooney, Polymeric tissue adhesives, Chem. Rev. 121 (18) (2021) 11336–11384.

[4] G.M. Taboada, K. Yang, M.J.N. Pereira, S.S. Liu, Y. Hu, J.M. Karp, N. Artzi, Y. Lee, Overcoming the translational barriers of tissue adhesives, Nat. Rev. Mater. 5 (4) (2020) 310–329.

[5] E.A. Yücel, O. Oral, V. Olgaç, C.K. Oral, Effects of fibrin glue on wound healing in oral cavity, J. Dent. 31 (8) (2003) 569–575.

[6] J. Wu, Z. Pan, Z.-Y. Zhao, M.H. Wang, L. Dong, H.L. Gao, C.Y. Liu, P. Zhou, L. Chen, C.J. Shi, Z.Y. Zhang, C. Yang, S.H. Yu, D.H. Zou, Anti-swelling, robust, and adhesive extracellular matrix-mimicking hydrogel used as Intraoral dressing, Adv. Mater. 34 (20) (2022) 2200115.

[7] R.E. Alexander, Dental extraction wound management: a case against medicating postextraction sockets, J. Oral Maxillofac. Surg. 58 (5) (2000) 538–551.

[8] S. Kumbargere Nagraj, E. Prashanti, H. Aggarwal, A. Lingappa, M.S. Muthu, S. Kiran Kumar Krishanappa, H. Hassan, Interventions for treating post-extraction bleeding, Cochrane, Db. Syst. Rev. 3 (2018) CD011930.

[9] D. Dudek, S. Marchionni, M. Gabriele, A. Iurlaro, K. Helewski, P. Toti, F. Gelpi, D. Bertossi, A. Barone, Bleeding rate after tooth extraction in patients under oral anticoagulant therapy, J. Craniofac. Surg. 27 (5) (2016) 1228–1233.

[10] E. Iwata, A. Tachibana, J. Kusumoto, T. Hasegawa, R. Kadoya, Y. Enomoto, N. Takata, M. Akashi, Risk factors associated with post-extraction bleeding in patients on warfarin or direct-acting oral anticoagulants: a retrospective cohort study, J. Oral Maxillofac. Surg. 26 (4) (2022) 641–648.

[11] D.J. Perry, T.J.C. Noakes, P.S. Helliwell, Guidelines for the management of patients on oral anticoagulants requiring dental surgery, Br. Dent. J. 203 (7) (2007) 389–393.

[12] W.L. Tan, T.L.T. Wong, M.C.M. Wong, N.P. Lang, A systematic review of post-extractional alveolar hard and soft tissue dimensional changes in humans, Clin. Oral Implants Res. 23 (Suppl 5) (2012) 1–21.

[13] F. Van der Weijden, F. Dell'Acqua, D.E. Slot, Alveolar bone dimensional changes of post-extraction sockets in humans: a systematic review, J. Clin. Periodontol. 36 (12) (2009) 1048–1058.

[14] R. Farina, L. Trombelli, Wound healing of extraction sockets, Endod. Top. 25 (2011) 16–43.

[15] M.G. Araújo, C.O. Silva, M. Misawa, F. Sukekava, Alveolar socket healing: what can we learn? Periodontol 2000 68 (1) (2015) 122–134.

[16] A.J. Eskow, B.L. Mealey, Evaluation of healing following tooth extraction with ridge preservation using cortical versus cancellous freeze-dried bone allograft, J. Periodontol. 85 (4) (2014) 514–524.

[17] H.J. Haugen, S.P. Lyngstadaas, F. Rossi, G. Perale, Bone grafts: which is the ideal biomaterial? J. Clin. Periodontol. 46 (S21) (2019) 92–102.

[18] A.S. Kalsi, J.S. Kalsi, S. Bassi, Alveolar ridge preservation: why, when and how, Br. Dent. J. 227 (4) (2019) 264–274.

[19] J.T. Gu, K. Jiao, J. Li, J.F. Yan, K.Y. Wang, F. Wang, Y. Liu, F.R. Tay, J.H. Chen, L. N. Niu, Polyphosphate-crosslinked collagen scaffolds for hemostasis and alveolar bone regeneration after tooth extraction, Bioact. Mater. 15 (2022) 68–81.

[20] W. Zhang, M. Yu, Y. Cao, Z. Zhuang, K. Zhang, D. Chen, W. Liu, J. Yin, An anti-bacterial porous shape memory self-adaptive stiffened polymer for alveolar bone regeneration after tooth extraction, Bioact. Mater. 21 (2023) 450–463.

[21] Z. Wang, Y. Zhang, Y. Yin, J. Liu, P. Li, Y. Zhao, D. Bai, H. Zhao, X. Han, Q. Chen, High-strength and injectable supramolecular hydrogel self-assembled by monomeric nucleoside for tooth-extraction wound healing, Adv. Mater. 34 (2022) 2108300.

[22] S. Li, L. Zhi, Q. Chen, W. Zhao, C. Zhao, Reversibly adhesive, anti-swelling and antibacterial hydrogels for tooth-extraction wound healing, Adv. Healthcare Mater. 13 (2024) 2400089.

[23] L. Chen, M. Peng, J. Zhou, X. Hu, Y. Piao, H. Li, R. Hu, Y. Li, L. Shi, Y. Liu, Supramolecular photothermal cascade nano-reactor enables photothermal effect, cascade reaction, and in situ hydrogelation for biofilm-associated tooth-extraction wound healing, Adv. Mater. 35 (2023) 2301664.

[24] Y. Liang, J. He, B. Guo, Functional hydrogels as wound dressing to enhance wound healing, ACS Nano 15 (8) (2021) 12687–12722.

[25] S. Li, Y. Xian, G. He, L. Chen, Z. Chen, Y. Hong, C. Zhang, D. Wu, In situ injectable Tetra-PEG hydrogel bioadhesive for sutureless repair of gastrointestinal perforation, Chin. J. Chem. 41 (2023) 3339–3348.

[26] J. Zhu, H. Zhou, E.M. Gerhard, S. Zhang, F.I. Parra Rodríguez, T. Pan, H. Yang, Y. Lin, J. Yang, H. Cheng, Smart bioadhesives for wound healing and closure, Bioact. Mater. 19 (2023) 360–375.

[27] H. Ren, Z. Zhang, X. Cheng, Z. Zou, X. Chen, C. He, Injectable, self-healing hydrogel adhesives with firm tissue adhesion and on-demand biodegradation for sutureless wound closure, Sci. Adv. 9 (33) (2023) eadh4327.

[28] R. Pinnaratip, M.S.A. Bhuiyan, K. Meyers, R.M. Rajachar, B.P. Lee, Multifunctional biomedical adhesives, Adv. Healthcare Mater. 8 (11) (2019) 1801568.

[29] Z. Zhu, K. Zhang, Y. Xian, G. He, Z. Pan, H. Wang, C. Zhang, D. Wu, A choline phosphoryl-conjugated chitosan/oxidized dextran injectable self-healing hydrogel for improved hemostatic efficacy, Biomacromolecules 24 (2) (2023) 690–703.

[30] J. Shi, D. Wang, H. Wang, X. Yang, S. Gu, Y. Wang, Z. Chen, Y. Chen, J. Gao, L. Yu, J. Ding, An injectable hemostatic PEG-based hydrogel with on-demand dissolution features for emergency care, Acta Biomater. 145 (2022) 106–121.

[31] Y. Hong, F. Zhou, Y. Hua, X. Zhang, C. Ni, D. Pan, Y. Zhang, D. Jiang, L. Yang, Q. Lin, Y. Zou, D. Yu, D.E. Arnot, X. Zou, L. Zhu, S. Zhang, H. Ouyang, A strongly adhesive hemostatic hydrogel for the repair of arterial and heart bleeds, Nat. Commun. 10 (2019) 2060.

[32] S. Gu, H. Wang, Y. Wang, X. Wang, X. Liu, Y. Wang, P. Liu, J. Ding, L. Yu, Thermosensitive nanocomposite hydrogel composed of PVPylated poly(D,L-alanine) and laponite as an injectable and bioactive biomaterial, Chem. Eng. J. 466 (2023) 143128.

[33] H. Yuk, J. Wu, T.L. Sarrafian, X. Mao, C.E. Varela, E.T. Roche, L.G. Griffiths, C. S. Nabzdyk, X. Zhao, Rapid and coagulation-independent haemostatic sealing by a paste inspired by barnacle glue, Nat. Biomed. Eng. 5 (10) (2021) 1131–1142.

[34] S. Bian, L. Hao, X. Qiu, J. Wu, H. Chang, G.M. Kuang, S. Zhang, X. Hu, Y. Dai, Z. Zhou, F. Huang, C. Liu, X. Zou, W. Liu, W.W. Lu, H. Pan, X. Zhao, An injectable rapid-adhesion and anti-swelling adhesive hydrogel for hemostasis and wound sealing, Adv. Funct. Mater. 32 (46) (2022) 2207741.

[35] H. Wang, J. Cheng, F. Sun, X. Dou, J. Liu, Y. Wang, M. Li, J. Gao, X. Liu, X. Wang, F. Yang, Z. Zhu, H. Shen, L. Zhang, P. Tang, D. Wu, A super tough, rapidly biodegradable, ultrafast hemostatic bioglue, Adv. Mater. 35 (10) (2023) 2208622.

[36] Y. Bu, L. Zhang, G. Sun, F. Sun, J. Liu, F. Yang, P. Tang, D. Wu, Tetra-PEG based hydrogel sealants for in vivo visceral hemostasis, Adv. Mater. 31 (28) (2019) 1901580.

[37] J. Li, A.D. Celiz, J. Yang, Q. Yang, I. Wamala, W. Whyte, B.R. Seo, N.V. Vasilyev, J. J. Vlassak, J. Suo, D.J. Mooney, Tough adhesives for diverse wet surfaces, Science 357 (6349) (2017) 378–381.

[38] Z. Ma, G. Bao, J. Li, Multifaceted design and emerging applications of tissue adhesives, Adv. Mater. 33 (24) (2021) 2007663.

[39] S. Wu, X. Zhao, Bioadhesive technology platforms, Chem. Rev. 123 (24) (2023) 14084–14118.

[40] R.M. Mendes, G.A.B. Silva, M.F. Lima, M.V. Calliari, A.P. Almeida, J.B. Alves, A. J. Ferreira, Sodium hyaluronate accelerates the healing process in tooth sockets of rats, Arch. Oral Biol. 53 (12) (2008) 1155–1162.

[41] T. Puidokas, M. Kubilius, D. Nomeika, G. Januzis, E. Skrodeniene, Comparative analysis of blood clot, plasma rich in growth factors and platelet-rich fibrin resistance to bacteria-induced fibrinolysis, Microorganisms 7 (9) (2019) 328.

[42] N. Laurens, P. Koolwijk, M.P.M. De Maat, Fibrin structure and wound healing, J. Thromb. Haemost. 4 (5) (2006) 932–939.

[43] J.M. Reinke, H. Sorg, Wound repair and regeneration, Eur. Surg. Res. 49 (2012) 35–43.

[44] B. Guo, R. Dong, Y. Liang, M. Li, Haemostatic materials for wound healing applications, Nat. Rev. Chem 5 (11) (2021) 773–791.

[45] H. Schell, G.N. Duda, A. Peters, S. Tsitsilonis, K.A. Johnson, K. Schmidt-Bleek, The haematoma and its role in bone healing, J. Exp. Orthop. 4 (1) (2017) 5.

[46] T. Sakai, T. Matsunaga, Y. Yamamoto, C. Ito, R. Yoshida, S. Suzuki, N. Sasaki, M. Shibayama, U. Chung, Design and fabrication of a high-strength hydrogel with ideally homogeneous network structure from tetrahedron-like macromonomers, Macromolecules 41 (14) (2008) 5379–5384.

[47] M. Farahani, A. Shafiee, Wound healing: from passive to smart dressings, Adv. Healthcare Mater. 10 (16) (2021) 2100477.

[48] Q. Zeng, X. Qi, G. Shi, M. Zhang, H. Haick, Wound dressing: from nanomaterials to diagnostic dressings and healing evaluations, ACS Nano 16 (2) (2022) 1708–1733.

[49] H. Montazerian, E. Davoodi, A. Baidya, S. Baghdasarian, E. Sarikhani, C.E. Meyer, R. Haghniaz, M. Badv, N. Annabi, A. Khademhosseini, Engineered hemostatic biomaterials for sealing wounds, Chem. Rev. 122 (2022) 12864–12903.

[50] H. Zhang, T. Zhao, P. Duffy, Y. Dong, A.N. Annaidh, E. O'Cearbhaill, W. Wang, Hydrolytically degradable hyperbranched PEG-polyester adhesive with low swelling and robust mechanical properties, Adv. Healthcare Mater. 4 (15) (2015) 2260–2268.

[51] N. Annabi, Y.N. Zhang, A. Assmann, E.S. Sani, G. Cheng, A.D. Lassaletta, A. Vegh, B. Dehghani, G.U. Ruiz-Esparza, X. Wang, Engineering a highly elastic human protein-based sealant for surgical applications, Sci. Transl. Med. 9 (410) (2017) eaai7466.

[52] X. Chen, J. Zhang, G. Chen, Y. Xue, J. Zhang, X. Liang, I.M. Lei, J. Lin, B.B. Xu, J. Liu, Hydrogel bioadhesives with extreme acid-tolerance for gastric perforation repairing, Adv. Funct. Mater. 32 (29) (2022) 2202285.

[53] N. Lang, M.J. Pereira, Y. Lee, I. Friehs, N.V. Vasilyev, E.N. Feins, K. Ablasser, E. D. O'Cearbhaill, C. Xu, A. Fabozzo, A blood-resistant surgical glue for minimally invasive repair of vessels and heart defects, Sci. Transl. Med. 6 (218) (2014) 218ra6.

[54] M. Chiquet, C. Katsaros, D. Kletsas, Multiple functions of gingival and mucoperiosteal fibroblasts in oral wound healing and repair, Periodontol 68 (1) (2015) 21–40, 2000.

[55] H. Lin, J. Sohn, H. Shen, M.T. Langhans, R.S. Tuan, Bone marrow mesenchymal stem cells: aging and tissue engineering applications to enhance bone healing, Biomaterials 203 (2019) 96–110.

[56] S. Viguet-Carrin, P. Garnero, P.D. Delmas, The role of collagen in bone strength, Osteoporosis Int. 17 (3) (2006) 319–336.

[57] D.J. Hadjidakis, I.I. Androulakis, Bone remodeling, Ann. Ny. Acad. Sci. 1092 (1) (2006) 385–396.

[58] J. Filipowska, K.A. Tomaszewski, Ł. Niedźwiedzki, J.A. Walocha, T. Niedźwiedzki, The role of vasculature in bone development, regeneration and proper systemic functioning, Angiogenesis 20 (3) (2017) 291–302.

[59] M. Marenzana, T.R. Arnett, The key role of the blood supply to bone, Bone Res 1 (1) (2013) 203–215.